Gallery of Fluid Motion

Rotation rate affects meltwater plumes below spinning ice disks

Kari Perry and Sarah Morris*
Montana State University, Bozeman, Montana 59717, USA

(Received 30 May 2025; published 20 November 2025)

This paper is associated with a poster winner of a 2024 American Physical Society's Division of Fluid Dynamics (DFD) Milton Van Dyke Award for work presented at the DFD Gallery of Fluid Motion. The original poster is available online at the Gallery of Fluid Motion, https://doi.org/10.1103/APS.DFD.2024.GFM.P2676604.

DOI: 10.1103/4swz-y3ww

As ice sheets and glaciers melt in the polar regions, icebergs break off and float throughout the oceans. Icebergs typically drift under the influence of ocean currents, strong winds and Coriolis forces; however, the world's largest iceberg, named A23a, was recently affected by another oceanic feature. In April of 2024, A23a drifted into a rotating Taylor column off the coast of Antarctica, which caused the iceberg to spin at a rate of 15° degrees per day [1]. A23a remained spinning for 9 months until it drifted out of the Taylor column in December of 2024.

The water tied up in icebergs accounts for half of the freshwater discharged from ice sheets annually [2]. Iceberg meltwater can adversely affect ocean systems, including slowing the global overturning circulation [3] and accelerating nutrient cycling [4]. Despite this, current climate models often underpredict ice melting [5], necessitating laboratory experiments on melting ice that can improve iceberg parametrizations in climate models [6,7]. Previous studies indicate that the meltwater below spinning ice disks influences surrounding fluid motions and therefore ice melt dynamics [8,9]. Inspired by A23a, this work conducts experiments on idealized, rotating, melting ice disks to study the effects of rotation on meltwater structures and ice melt rates. Flow visualization (FV) experiments in Fig. 1 illuminate the meltwater structures below melting ice disks for three different rotation rates.

Experiments are conducted in a large tank ($46 \times 46 \times 46$ cm), shown in Fig. 2 (left), filled with quiescent freshwater at room temperature (20 °C) and with density $\rho = 998$ kg/m^3. The Prandtl number describes the ratio of momentum to thermal diffusivity, $\mathrm{Pr} = \nu/\alpha$, where ν is kinematic viscosity and α is thermal diffusivity. In these experiments, $\nu = 1.00 \times 10^{-6}$ m^2/s and $\alpha = 1.43 \times 10^{-7}$ m^2/s giving $\mathrm{Pr} = 7$. To make ice disks, fluorescein dye is mixed with freshwater (0.01% fluorescein by volume) and frozen overnight to −18 °C in cylindrical molds measuring $h_0 = 3.18$ cm in height and $D_0 = 6.35$ cm in diameter, giving an initial ice aspect ratio of $h_0/D_0 = 0.5$. This aspect ratio is within the range for natural icebergs, $h/D = 0.001$–1 [7]. Ice disks are mounted to a rotation platform by freezing a threaded nylon rod into the top of the ice disk. A stepper motor and radial encoder rotate the ice disks, shown in Fig. 2 (right), at steady rotation rates $\omega = 0°/\mathrm{s}$, 13.7°/s, and 27.5°/s.

*Contact author: sarah.morris14@montana.edu

Published by the American Physical Society under the terms of the Creative Commons Attribution 4.0 International license. Further distribution of this work must maintain attribution to the author(s) and the published article's title, journal citation, and DOI.



FIG. 1. Meltwater plumes below spinning ice disks for rotation rates: (left) $\omega = 0^\circ/\text{s}$, (middle) $\omega = 13.7^\circ/\text{s}$, and (right) $\omega = 27.5^\circ/\text{s}$. Images are placed side by side in a single panel in postprocessing and a transparent-to-black gradient is added to the bottom of the panel.

During flow visualization (FV) experiments, the ice meltwater fluoresces green under a 470-nm volumetric floodlight (Thorlabs SOLIS-470C). The tank walls are covered with blackout foam to eliminate reflections and minimize background convective currents. The scene is captured with a digital single-lens reflex camera (Canon EOS) with a shutter speed of 0.0025 s, frame rate of 24 Hz, and resolution of 3840 × 2160 pixels (31 × 17 cm). Images are recorded starting at time $t = 1$ min after the ice disk is lowered into the tank to allow the meltwater structures to propagate along the full height of the field of view. The experiments run for an additional 3 min from $t = 1$ min to $t = 4$ min before removing the ice disks from the tank. Ice melt rate is reported as the mass loss over an experiment $\Delta m = (m_0 - m_f)$, where initial mass m_0 and final mass m_f are taken at $t = 0$ min and $t = 4$ min, respectively, and measured using a digital bench-top scale with ± 0.1 g accuracy.

A "plume" describes one fluid continuously emitted into another [10]; in these experiments, the plume is formed by meltwater being emitted into ambient water, seen in Fig. 3. These plumes are negatively buoyant as the cold meltwater is denser than the ambient water, causing the plume to flow downward. Near the ice base, the local vertical velocity increases and the plume contracts due to continuity. Rayleigh-Taylor instabilities can arise at the boundary of the plume and ambient water, which drives turbulent entrainment of ambient water into the plume and can lead to "puffing instabilities" [11]. "Puffs" describe the vortical structures that periodically pulse from a plume due to the interaction of the buoyant body force due to density disparities, and radial stretching force due to source rotation [11,12].

The near-field plume is identified between $0 < z \leqslant D_0$ where z is the height below the ice base. Without rotation ($\omega = 0^\circ/\text{s}$), the near-field plume is narrow and there is minimal turbulent entrainment of ambient water. In the far field ($z > D_0$), puffs develop. This is shown at several instances for $\omega = 0^\circ/\text{s}$ in Fig. 3, where puffing arises in the far field while the near field remains stable.

Under rotation, the ice disk can be modeled as a von Kármán rotating disk [13], which produces swirling flow in the plume associated with rotation. Swirling flow is expected to enhance turbulence [14] leading to puff deformation, increased fluid entrainment, and plume expansion. This is first seen for $\omega = 13.7^\circ/\text{s}$ in Fig. 1 (middle) where the plume widens under the centrifugal force and

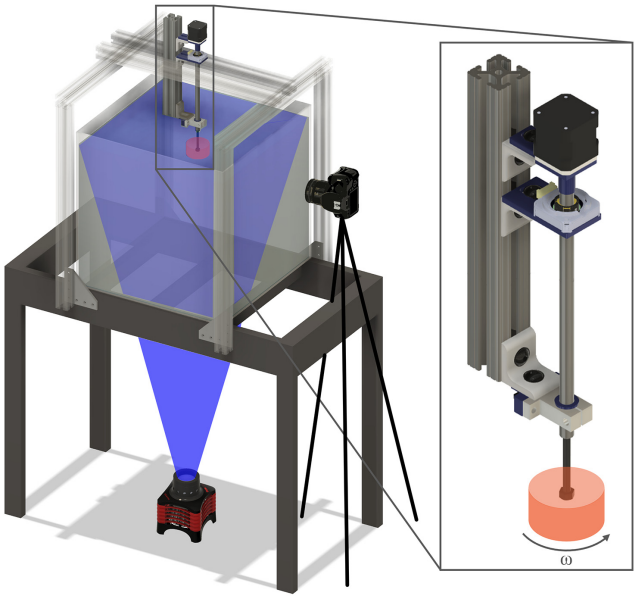


FIG. 2. Left: Model of the test environment. samples are mounted to a rotation platform above a quiescent tank. A floodlight is positioned below the tank and a camera captures the vertical flow profiles from the samples. Right: Model of the rotation platform and initial ice sample.

puffs develop close to the ice base. For $\omega = 27.5^\circ/\text{s}$, the plume further expands radially as larger puffs are released from the ice base and mixing increases, shown in Fig. 1 (right).

The plumes are fed by the boundary layer of meltwater that forms along the ice surface and flows toward the center of the ice base. The plume source width is governed by the radial distance of the flow separation points, where the boundary layer flow detaches from the ice surface. The separation radius b_{sep} is measured from the time-averaged FV images, shown for $\omega = 0^\circ/\text{s}$ in the rightmost panel of Fig. 3. The time-averaged plume is binarized, and the first and last nonzero pixels along the first row below the ice base are taken as the left and right separation points, respectively.



FIG. 3. Instantaneous flow visualization images of an ice disk for $\omega = 0^\circ/\text{s}$ from one sample at (left to right) times $t = 2$, 3, and 4 min, and time averaged. Images are placed side by side in a single panel in postprocessing. Crosses ($\times$) indicate the time-averaged flow separation points.

At the flow separation points, the negatively buoyant body force overcomes the viscous force adhering the boundary layer flow to the ice surface. When rotation is added, the inward boundary layer flow is opposed by the outward centrifugal force proportional to ω. As a result, b_{sep} is found to increase (move outward) with ω ($b_{sep}/D_0 = 0.235, 0.309, 0.436$ for $\omega = 0^\circ/s, 13.7^\circ/s, 27.5^\circ/s$, respectively). Flow separation directly affects local convection by encouraging fluid entrainment of ambient water into the near-field plume, increasing melting [15]. As b_{sep} increases, entrainment occurs over a larger area of the ice base and melt rates increase ($\Delta m/m_0 = 0.508, 0.512, 0.570$ with a maximum standard deviation of ± 0.05, for $\omega = 0^\circ/s, 13.7^\circ/s, 27.5^\circ/s$, respectively). This is supported by previous work that found ice melt rates increase with increased turbulence intensity [16].

In summary, this work characterizes the meltwater structures below spinning ice disks as negatively buoyant plumes and quantifies the effect of rotation on b_{sep} and Δm using flow visualization. For $\omega = 0^\circ/s$, the meltwater forms a narrow negatively buoyant plume with minimal turbulent entrainment in the near field. As ω increases, the plume widens and puffs of meltwater are released from the ice base. As ω increases, the plume exhibits swirling flow, b_{sep} increases under the rotation-induced centrifugal force that opposes the meltwater boundary layer flow, and $\Delta m/m_0$ increases due to local convection driven by flow separation and ambient fluid entrainment.

These findings support the greater goal of improving iceberg parametrizations in climate models by studying the fundamental flow dynamics of melting ice. These experiments make several simplifications that differ from natural icebergs; for example, the ambient flow is quiescent and ice rotation is constrained to one axis, which are idealized conditions but allow the effect of rotation to be isolated for study. In nature, meltwater plumes from icebergs are highly complex and are affected by additional factors such as ambient temperature, salinity and ocean currents. Future work will quantify the meltwater plume characteristics and consider how they affect local melt dynamics of spinning ice disks.

ACKNOWLEDGMENT

This material is based upon work supported by the National Science Foundation Graduate Research Fellowship Program under Grant No. 2439625.

DATA AVAILABILITY

The data that support the findings of this article are not publicly available upon publication because it is not technically feasible and/or the cost of preparing, depositing, and hosting the data would be prohibitive within the terms of this research project. The data are available from the authors upon reasonable request.

[1] J. Amos and E. Rivault, World's biggest iceberg spins in ocean trap, BBC News [London, U.K.] (2024).

[2] M. A. Depoorter, J. L. Bamber, J. A. Griggs, J. T. M. Lenaerts, S. R. M. Ligtenberg, M. R. van den Broeke, and G. Moholdt, Calving fluxes and basal melt rates of antarctic ice shelves, Nature (London) **502**, 89 (2013).

[3] M. Srokosz, M. Baringer, H. Bryden, S. Cunningham, T. Delworth, S. Lozier, J. Marotzke, and R. Sutton, Past, present, and future changes in the atlantic meridional overturning circulation, Bull. Am. Meteorol. Soc. **93**, 1663 (2012).

[4] L. P. A. M. Duprat, G. R. Bigg, and D. J. Wilton, Enhanced Southern Ocean marine productivity due to fertilization by giant icebergs, Nat. Geosci. **9**, 219 (2016).

[5] D. A. Sutherland, R. H. Jackson, C. Kienholz, J. M. Amundson, W. P. Dryer, D. Duncan, E. F. Eidam, R. J. Motyka, and J. D. Nash, Direct observations of submarine melt and subsurface geometry at a tidewater glacier, Science **365**, 369 (2019).
[6] A. McCutchan and B. Johnson, Laboratory experiments on ice melting: A need for understanding dynamics at the ice-water interface, J. Mar. Sci. Eng. **10**, 1008 (2022).
[7] C. Cenedese and F. Straneo, Icebergs melting, Annu. Rev. Fluid Mech. **55**, 377 (2023).
[8] S. Dorbolo, N. Adami, C. Dubois, H. Caps, N. Vandewalle, and B. Darbois-Texier, Rotation of melting ice disks due to melt fluid flow, Phys. Rev. E **93**, 033112 (2016).
[9] L. M. Schellenberg, T. J. Newton, and G. R. Hunt, On the rotation of melting ice disks, Environ. Fluid Mech. **23**, 465 (2023).
[10] G. R. Hunt and T. S. van den Bremer, Classical plume theory: 1937–2010 and beyond, IMA J. Appl. Math. **76**, 424 (2011).
[11] B. M. Cetegen and K. D. Kasper, Experiments on the oscillatory behavior of buoyant plumes of helium and helium-air mixtures, Phys. Fluids **8**, 2974 (1996).
[12] M. V. Pham, F. Plourde, and S. D. Kim, Unstable process identification in a pure thermal plume under forced rotating conditions, Exp. Heat Transfer **24**, 151 (2011).
[13] T. Von Kármán, On laminar and turbulent friction, J. Appl. Math. Mech. **1**, 233 (1921).
[14] M. V. Pham, F. Plourde, S. D. Kim, and S. Balachandar, Large-eddy simulation of a pure thermal plume under rotating conditions, Phys. Fluids **18**, 015101 (2006).
[15] R. Yang, T. van den Ham, R. Verzicco, D. Lohse, and S. G. Huisman, Circular objects do not melt the slowest in water, Phys. Rev. Fluids **9**, 083501 (2024).
[16] A. L. McCutchan, C. R. Meyer, and B. A. Johnson, Enhancement of ice melting in isotropic turbulence, Phys. Rev. Fluids **9**, 074601 (2024).